Testing the spin-current source of gravity

Can a measured current predict a galaxy's speed?

The question raised in the latest ESFD discussions is whether a spin field can predict both the location and the strength of extra gravity before a galaxy's rotation curve is known. Christopher Grenke's proposed source is the divergence of an entropy-weighted spin current. This study tests whether neutral hydrogen transports the relevant spin and entropy in fixed proportion to its mass. That assumption makes the current measurable up to one shared coefficient.

> For NGC 2403 the gas-current model predicts 57.3 km/s at 16.89 kpc. The measured speed is 134.0 km/s. Its predicted excess gravity peaks toward the inner edge of the tested region, while the required excess in squared speed peaks at the outer edge.

Question	Result
Does measured radial gas flow supply the missing gravity?	Across eight galaxies and 115 outer speed measurements, the mean per-galaxy error is 78.6 km/s. Ordinary matter alone gives 80.3 km/s.
Does the empirical mass-based equation still transfer?	Across 255 external galaxies, the frozen slower-rise model gives 32.76 km/s against 66.82 km/s for ordinary matter. A pseudo-isothermal halo with the same mass scaling gives identical predictions.
Can lensing distinguish model branches?	Fitting a constant response to light on other mass bins leaves far-field errors of 78.3 and 28.1 km/s for the two previously calibrated branches.
Which earlier calculation can be completed?	The causal-diamond boundary is now solved through face overlap and complete spatial coverage. Its integrated area recovers the exact volume of the quotient space.

The accompanying register revisits each of the 75 earlier branches and adds the completed geometry calculation. It records which equations, calibrations or observations would discriminate the remaining claims. The source of gravity and the mechanism that would hold a real galaxy at critical spin response remain open.

Observational basis · Radial H I flow measurements · SPARC · Weak lensing. Equations and interpretation · ESFD source manuscripts and preceding studies in this master.

What the source equation actually fixes

Write $\rho_x = \nabla\cdot Q$ and $\nabla^2\Psi_x = 4\pi G\rho_x$, with the phenomenological normalization absorbed into Q. Its units are mass per area. Around a finite isolated source, collisionless tracers respond to the gravitational potential Ψ. For an axisymmetric current with only an azimuthal component the divergence vanishes, even if the azimuthal flow is large. Ordered rotation alone therefore supplies no source in this equation.

A closure that can be tested without using the target speeds

Let $Q_R = \tau\rho_{HI}u_R$, with a signed conversion time τ and radial gas speed u_R positive outward. Assume axial symmetry, a regular center and vanishing flux through the upper and lower disk faces. Define $F(R) = 2\pi R\int\rho_{HI}u_R\,dz$. Vertical integration of the divergence and then integration over the disk give two exact identities for this closure.

> $\Sigma_x(R) = \tau\,F'(R)/(2\pi R)$ and $M_x^{cyl}(<R) = \tau\,F(R)$.

A radially constant flow contributes no local source within that annulus. Where the flow returns to zero, the cumulative excess mass also returns to zero. A compensated disk can still exert a force inside it. The calculation integrates the force of signed annuli, including matter outside the test radius. Treating this disk as a sphere would change the prediction.

The ideal, infinitely extended Mestel disk has $\Sigma = V^2/(2\pi GR)$ and constant circular speed V. For this particular disk the required flow gradient is $F' = V^2/(G\tau)$. This is a diagnostic for a constant excess speed. The forward test on the next page uses the measured F(R) point by point. Its input contains no flat-speed condition.

What remains invisible to rotation

Adding the curl of any regular vector potential to Q leaves ρ_x unchanged. Compact support preserves the boundary flux as well. If Q is the product of specific spin entropy and a spin current, multiplying one factor by an arbitrary positive function and dividing the other by it also preserves Q. Separate transport or spin measurements are necessary to recover the factors. Circular speeds constrain still less, because they sample one derivative of a potential on the disk.

ESFD · current-divergence branch and November source reconciliation. Thin-disk comparison · Mestel, On the Galactic Law of Rotation. Gas flow convention · Schmidt et al..

NGC 2403 gives a test of location and strength

Schmidt and colleagues published 54 radial H I mass-flow measurements for NGC 2403. Reading the centers and uncertainty bars of their vector plot recovers an outer mean of −1.196 M/yr, agreeing with their tabulated −1.20 M/yr. Of those 54 rings, 33 lie outside the optical radius. At the SPARC distance of 3.16 Mpc the common outer interval contains 20 circular-speed observations from 7.45 to 16.89 kpc.

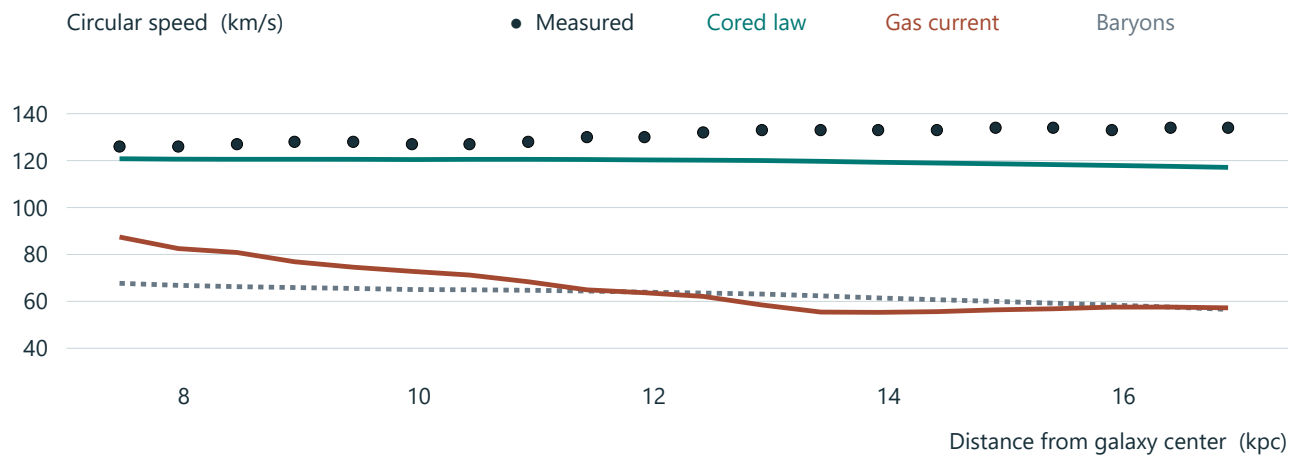

The signed conversion fitted on the other seven galaxies is $\tau = -0.709$ Gyr. Its sign describes how the proposed gravitational charge would follow an inflow. It does not measure a gas travel time. The predicted excess in squared speed reaches its maximum at 7.45 kpc. The required excess reaches its maximum at 16.89 kpc. Their Pearson correlation across these 20 radii is −0.84. Neighboring radii share errors, so this is descriptive.

The median required excess is 13,099 $(\mathrm{km/s})^2$. The median predicted excess is 33 $(\mathrm{km/s})^2$. As a scale check, the ideal flat-disk gradient from the preceding page is −4.29 M/yr/kpc, while the measured gradient across the 31 flux rings between the first and last speed measurements is +0.31 M/yr/kpc. The disk integral in the figure uses the full measured profile and its outer continuation.

The gas-current speed RMSE is 65.98 km/s. Baryons give 67.84 km/s and the archived, separately calibrated cored curve gives 11.55 km/s on these same radii. Replacing every observed NGC 2403 speed with zero leaves its forward current prediction exactly unchanged. The two surveys can share gas geometry and line-of-sight systematics.

Measurements · Schmidt et al., figure 8 and table 1 · SPARC mass models and rotation curves. Reproduction · forward_current/results/held_predictions.csv and force_locations.csv.

Eight galaxies test whether the calibration transfers

The ten published flow profiles contain 304 rings. Their reconstructed optical-exterior means agree with all ten tabulated rates to within 0.006 M/yr. Eight galaxies enter the archived SPARC selection. NGC 925 and NGC 3621 have measured flows and lack a curve in this 131-galaxy cut. Every included galaxy has at least two outer speed points inside its mapped flow extent. Six of the eight have mean inflow, and two have mean outflow. All eight have a positive median spherical-equivalent excess mass. Its sign alone cannot determine the disk force.

Eight held galaxies	Mean speed RMSE (km/s)	Mean squared-speed RMSE ((km/s)^2)
Baryons	80.34	25,897
Signed measured flow plus baryons	78.63	25,427
Constant excess in squared speed, trained on other galaxies	30.34	12,215
Archived cored model, calibrated on other SPARC folds	20.20	8,750

Each speed score is an average of eight galaxy-level errors. Each current coefficient is fitted on the other galaxies using squared speeds and equal galaxy weight. The finite disk model has a 0.5 kpc gravitational softening length and returns the measured flux to zero over 5 kpc beyond the last ring. Changing the softening to 0.25 or 1 kpc gives 79.10 or 77.24 km/s. Changing the taper to 2 or 10 kpc gives 77.98 or 79.43 km/s.

NGC 6946 has a nearly face-on geometry and a particularly uncertain flow. Excluding it from training and testing reverses the small advantage over baryons on squared speeds and produces one negative predicted speed square. Taking absolute flow also gives one such point. Shifting all rings coherently by their reported errors yields two or eighteen invalid speeds. These are stress tests. The paper's quoted outer uncertainty is an average ring uncertainty, and published ring covariances are unavailable.

Three galaxies also have H I intensity maps and total-disk radio field estimates. On their 28 common outer speeds, the measured-flow model gives 65.92 km/s, radio weighting gives 66.23, and a constant-drift model using the gas density map gives 55.71. A fitted constant offset gives 11.08. A mean equipartition field supplies no radial measurement of the ordered spin current.

THINGS gas flows · HALOGAS maps · Radio field estimates. Numerical tables include scores, sensitivity variants, disk assumptions and sign conventions.

What survives the larger galaxy comparison

The archive contains 3,032 SPARC rows in 131 galaxies, 16,120 PROBES rows in 245 and 706 LITTLE THINGS rows in 17. That is 19,858 velocity rows across 393 catalog entries. Seven dwarfs coincide on the sky with entries in the wider SPARC catalog. Removing them leaves 386 curves and 19,413 rows. The earlier count of 19,008 designates distinct galaxy–radius pairs in SPARC plus PROBES. Some two-sided measurements share a radius.

> $v^2 = v_b^{\,2} + \sqrt{(GM_b a_*)}\,[1 - \arctan(x)/x]$, $x = R/(0.679624\,R_d)$, $a_* = 1.163796 \times 10^{-10}$ m/s².

Model	Frozen parameters, 255 external galaxies	Matched refit, 386 galaxies
Ordinary matter	66.82	60.55
Slower-rise empirical law	32.76	27.95
Revised cored law	33.73	28.11
Radial acceleration relation	33.60	28.40
Shared NFW / Burkert profiles	See matched refit	28.15 / 28.94

Values are mean per-galaxy RMSE in km/s. The frozen column uses the latest slower-rise coefficients and the older archived core and radial-acceleration calibrations. Including all 17 dwarfs gives 32.17 km/s for the frozen slower-rise law, consistent to 0.01 with the chat's 32.16. Its 27.38 km/s combined score and 32.9 km/s core score use a different calibration. The full benchmark file linked in that chat was unavailable. The matched refit here minimizes mean galaxy RMSE on the same SPARC training partitions for each profile. The paired slower-rise advantage over RAR is 0.45 km/s, with a conditional galaxy-bootstrap interval of 0.12–0.76 km/s.

For a spherical pseudo-isothermal halo, $\rho = \rho_0/(1+x^2)$ gives $M(<R) = 4\pi\rho_0 r_c^{\,2}[R - r_c \arctan(x)]$. Set $4\pi G\rho_0 r_c^{\,2} = \sqrt{(GM_b a_*)}$ and use the same r_c. The two curves then agree at every radius. Computing both expressions separately across all 19,858 rows gives a maximum difference below 10^{-12} km/s. The scaling transfers. Deciding which physics sets that scaling requires an independent observable.

SPARC · PROBES · LITTLE THINGS · Empirical radial acceleration relation. Shared halo fits here use the declared baryonic mass and scale prescription.

What light and cosmic expansion add

Massive bodies in the weak field constrain the time potential Ψ. Lensing responds to the sum of Ψ and the spatial potential Φ. For this test only, let the extra components obey $\Phi_x = \eta_x \Psi_x$ with η_x constant. Keep the baryons at their usual response. The lensing-equivalent speed then satisfies $v_L^2 = v_b^2 + (1+\eta_x)v_x^2/2$. This effective relation assumes the same projected profiles and constant slip over the tested band.

For each excluded baryonic-mass bin, fit one coefficient on the 18 cells at 50–300 kpc in the other three bins. Predict the four cells at 300–1,000 kpc in the excluded bin. All 16 outer predictions use the rotation-calibrated carrier models from the preceding edition. This is a retrospective cross-bin check on published late-type galaxy stacks.

Carrier model	Unit response, outer RMSE	Fitted response, outer RMSE
Fixed microscopic stiffness	88.62 km/s	78.28 km/s
Critical stiffness retuned with carrier filling	28.61 km/s	28.09 km/s

The four fitted η_x values span 1.41–1.73 for fixed stiffness and 0.97–1.07 for retuned stiffness. A constant lensing rescaling does little to change the gap. The stacks share calibration uncertainties. The ranges across fits are descriptive. Deriving η_x requires field equations for both potentials.

Can the galaxy equation also drive cosmic acceleration?

A homogeneous, isotropic universe admits no preferred spatial current in its rest frame. More generally the integral of a regular spatial divergence over a closed spatial slice vanishes. The galaxy source by itself therefore supplies no homogeneous density through that term. A covariant four-divergence could include a time derivative. It requires an evolution law and a stress-energy tensor.

The acceleration equation involves $\rho + 3p/c^2$. An additive constant in a candidate generally covariant matter action shifts vacuum energy and pressure without fixing the galaxy current law. An equation of state, conservation law, background solution and perturbation behavior are necessary to compare this theory with expansion and structure measurements. The geometry on the next page can be calculated without choosing these quantities.

Mistele et al., lensing data and assumptions · Zhang et al., testing the metric potentials · Riess et al., supernova expansion measurements.

The causal diamond through complete coverage

Keep the archived static round metric with curvature radius R on the Poincaré dodecahedral space. Two events occur at the same spatial point separated by 2T. At the symmetry time the waist is the boundary of the geodesic ball reached by first arrival. Write $\chi = cT/R$ and $f = \pi/10$. Past the first face, each of the twelve face normals removes a cap from the sphere of directions with limiting cosine $u = \tan(f)/\tan(\chi)$. Adjacent normals have dot product $d = 1/\sqrt{5}$.

Between the face and first edge the surviving solid angle is $\Omega = 4\pi - 24\pi(1-u)$. The edge occurs at $\chi = 0.364864$. Beyond it, add the overlap of each of 30 adjacent cap pairs. Before full coverage there is no triple overlap with positive area. With $\theta = \arccos u$ and $\delta = \arccos d$, a single spherical lens has solid angle $L = 2\pi - 2\gamma - 4u\alpha$, where $\cos\alpha = \cot\theta \tan(\delta/2)$ and $\cos\gamma = (d-u^2)/(1-u^2)$. These angles follow from the spherical triangle between the two cap centers and one intersection point.

> Beyond the first edge, $A/R^2 = \sin^2\chi\,[4\pi - 24\pi(1-u) + 30L]$. At $\chi = \arctan[\tan(f)/\sqrt{((1+2d)/3)}] = 0.388140$ the slice is fully covered and its first-arrival boundary area is zero.

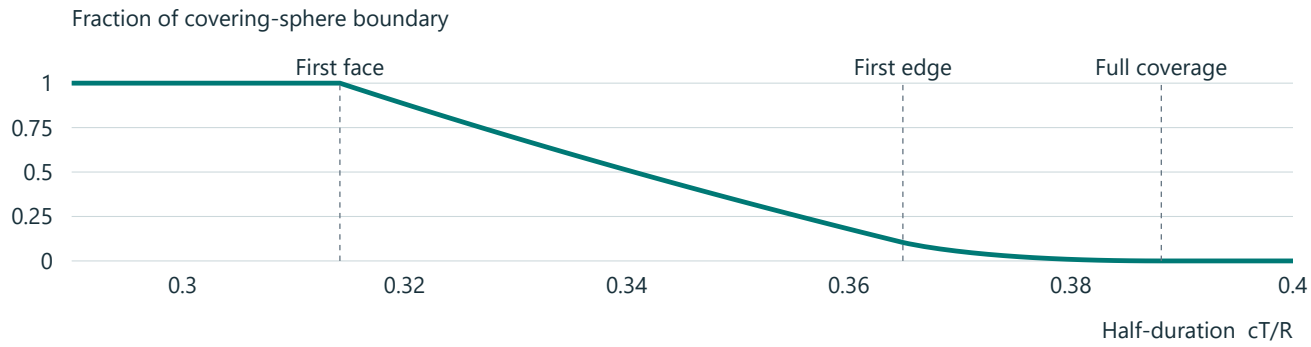

At $\chi = 0.348$ the original figure's surviving fraction is 0.374073. Integrating the new area through complete coverage gives $V/R^3 = 0.16449340668474$, agreeing with $2\pi^2/120$ to 9×10^{-14} in absolute units. A second calculation traces 150,000 directions and agrees within 0.00031 in surviving fraction. This completes the static geometric baseline. Establishing cosmic topology or spin dynamics requires observational predictions beyond that construction.

Geometry · Luminet et al., Poincaré dodecahedral space. Original marked figure · archived Pattern Nexus dodecahedron package. Independent implementations and checks · spin_entropy/diamond.py and diamond_checks.json.

What the complete project review resolves

The register preserves every earlier branch and its source, including proposed experiments with no calibrated signal. Its November 29 columns state the present result or the specific missing observable. The new geometry entry makes 76 entries. The separate equations for an empirical galaxy curve, an interface-mediated force and a current transported by gas have different physical inputs and different experimental tests.

Area	Result and remaining measurement
Critical spin response	The effective stiffness is $a_R - 4\pi G\lambda^2$ in the reciprocal coupling model. At zero stiffness a quartic spin energy gives $v \propto R^{1/6}$. A cubic energy from neutral two-dimensional interface modes can give $v_\infty{}^4 = GMa_D$. A galactic carrier census, gap or independently measured susceptibility would set the scale and test whether criticality persists.
Stars and pulsar timing	The original BΩ threshold using timing-inferred B ranks inverse characteristic age. Five of 22 eligible confirmed magnetars pass. For one star the earlier study also inferred a field from spectroscopy, subject to line identification and redshift. Independent fields and event exposure are required for a population test.
Material spin and laboratory tests	In the specified quartic reversible model the coefficients obey $c_1c_5 = 3c_3{}^2$. A four-state reversal removes additive offsets. Independent magnetometry, same-material sweeps and a phase-sensitive readout would distinguish joint-parity backgrounds and test the prediction.
Particles, compact objects and clocks	The Pauli operator and repaired clock diagnostic are specified. A clock Hamiltonian, collider interference coefficients and a conserved material or stellar stress tensor remain separate quantitative requirements.
Expansion and global spacetime	The spatial-divergence average vanishes on a closed slice. The static topology calculation is complete. A time-dependent source, pressure and exterior matching would be needed to predict accelerated expansion or a global bounce.

The 255-galaxy population result is the clearest transferable prediction in this revision. The resolved gas experiment now supplies a quantitative constraint on one proposed carrier of that gravity. A measurement of ordered spin polarization and its transport independent of the circular speeds could distinguish a different carrier from the halo-equivalent mass law.

McGill Magnetar Catalog · Independent stellar spectroscopy. Project references · branch_register.csv, spin_response/, stars/, critical_response/ and the preceding studies in this master.